Importance of the indirect exchange interaction via *s* states in altermagnetic HgMnO$_3$

Danil A. Myakotnikov [1,2] Evgenia V. Komleva [2,3] Youwen Long,[4] and Sergey V. Streltsov [2,3,*]

[1]*Department of Physics of Cumulative Processes, Ural Federal University, Mira Street 19, 620002 Ekaterinburg, Russia*
[2]*M. N. Mikheev Institute of Metal Physics UB RAS, S. Kovalevskaya Street 18, 620137 Ekaterinburg, Russia*
[3]*Department of Theoretical Physics and Applied Mathematics, Ural Federal University, Mira Street 19, 620002 Ekaterinburg, Russia*
[4]*Beijing National Laboratory for Condensed Matter Physics, Institute of Physics, Chinese Academy of Sciences, Beijing 100190, China*

The electronic and magnetic properties of a recently synthesized perovskite phase of HgMnO$_3$ are studied. By means of *ab initio* density functional theory calculations this material was shown to be altermagnetic. We discuss the features of its electronic structure and unveil the physical mechanism of the anomalous suppression of the antiferromagnetic exchange interaction in this material. While it is tempting to ascribe the unexpectedly weak exchange interaction between nearest neighbors to crystal structure distortions, this is an indirect ferromagnetic exchange via Hg $6s$ states, which strongly affects the magnetic properties. This effect can be important not only for HgMnO$_3$, but also for many other transition metal compounds having empty s states, placed not far above the Fermi level.

I. INTRODUCTION

The interest in manganese oxides with a perovskite crystal structure (commonly known as manganites) in the last three decades was mostly related to the discovery of colossal magnetoresistance in these materials [1,2] and multiferroicity [3]. Both these aspects are attributed to an interplay between different degrees of freedom, such as lattice, charge, spin, and orbital. This makes manganites extremely interesting not only from a theoretical point of view, but also as an important class of materials for applied physics, e.g., spintronics and the design of ferroelectromagnets [4–7].

The members of manganese perovskites' family demonstrate a rather rich phase diagram with magnetic properties changing from different types of antiferromagnetism to ferromagnetism depending on the number of d electrons and structural distortions (see, e.g., Ref. [8] for the phase diagram of La$_{1-x}$Ca$_x$MnO$_3$ series). Such a variety of their magnetic properties is commonly explained by the competition between two relevant interaction mechanisms, double exchange and superexchange [9], that stabilize either ferromagnetic or antiferromagnetic states.

Among other well-studied manganese oxides with a perovskite structure special attention has been paid to CaMnO$_3$. The crystal structure of CaMnO$_3$ possesses rhombohedral symmetry and is characterized by the *Pnma* space group [10]. This compound is a well-studied insulator [11]. The d levels of the Mn^{4+} $3d^3$ ion in an octahedral crystal field are split into e_g and t_{2g} subshells, with three electrons occupying the t_{2g} levels, giving a half-filled configuration. Therefore, strong antiferromagnetic coupling is expected in the case of CaMnO$_3$ due to the superexchange mechanism. Its Néel temperature is 125 K, and the Curie-Weiss temperature θ is approximately -500 K (antiferromagnetic) [12].

Interestingly, another manganite HgMnO$_3$, with the same Mn^{4+}, exhibits a much lower Néel temperature, which is around 60 K. Its Curie-Weiss temperature is -153 K [13].

In general, mercury-based manganites (both pure HgMnO$_3$ and doped with lead Hg$_{1-x}$Pb$_x$MnO$_3$) attract much interest due to the possibility of strong octahedral distortions resulting in a polar crystal structure and giving rise to giant electronic polarization and photovoltaic effects [14]. Moreover, it is natural to expect that distortions in the crystal structure are responsible for the strong modification of the exchange interaction.

HgMnO$_3$ is obtained through the reaction of HgO and MnO$_2$ at high temperatures (1473 K) and pressures (20 GPa) [13]. Under these conditions, the synthesized system has a rhombohedral crystal structure, the space group $R\bar{3}c$ (No. 167) [13]. HgMnO$_3$ is insulating and one might expect that, similar to CaMnO$_3$, it can be a G-type antiferromagnet. The crystal structures of these two materials are very similar, but it remains unclear what results in a lowering of Néel temperature in HgMnO$_3$ in comparison with the other manganese perovskites. Indeed, the d orbitals of Hg^{2+} ions are fully occupied, making the ions nonmagnetic. The exchange interaction between the half-filled t_{2g} orbitals of Mn atoms is expected to result in a strong antiferromagnetic exchange.

Our first-principles calculations unveil a physical mechanism for the suppression of the antiferromagnetic exchange in HgMnO$_3$. The presence of Hg s states not far above the Fermi level provides a ferromagnetic contribution to the exchange interaction via their hybridization with Mn e_g states. Such an effect results in the anomalous suppression of the magnetic transition temperature.

II. COMPUTATIONAL DETAILS

The experimental crystal structure from Ref. [13] was taken for the calculations. The unit cell used for the total

*Contact author: streltsov@imp.uran.ru
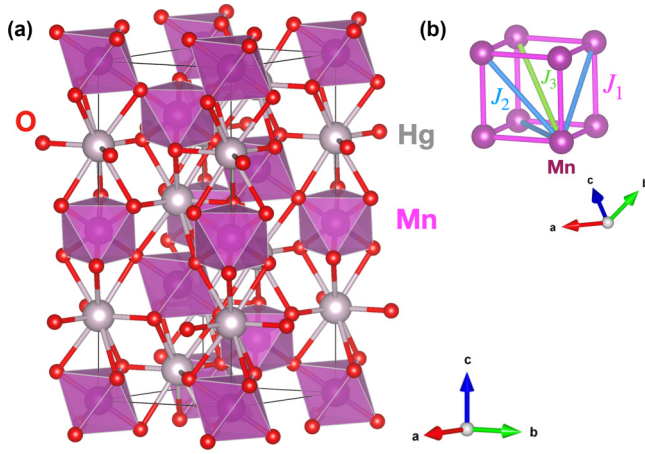
FIG. 1. (a) The crystal structure of HgMnO$_3$. Purple spheres represent Mn atoms surrounded by oxygen (red) octahedra, and gray spheres are mercury. (b) Scheme of the isotropic exchange paths J_1 (purple), J_2 (blue), and J_3 (light green) up to the third nearest neighbors drawn for one Mn atom in a cube.

FIG. 2. Total energy (ΔE) of the system relative to the minimum for different values of U. The trend of change for AFM-C is depicted in red, AFM-A in green, AFM-G in blue, and FM in purple. The inset plot shows an enlarged scale, since the values of ΔE at $U = 2.5$ and 3 eV between AFM-G and AFM-C are too small.

energy calculations contained six Hg atoms, six Mn atoms, and 18 O atoms [see Fig. 1(a)]. We employed the projector augmented-wave (PAW) implementation of the Vienna *ab initio* simulation package (VASP) [15–17]. Self-consistent calculations were carried out with the Perdew-Burke-Ernzerhof (PBE) version of the generalized gradient approximation (GGA) exchange-correlation functional [18]. The cutoff energy for the plane-wave basis set is 500 eV. We used a $6 \times 6 \times 2$ k-point mesh. The calculations were performed using the tetrahedron method with Blöchl corrections [19].

To take into account the correlation effects, the rotation-invariant density functional theory (DFT)+U method introduced by Liechtenstein *et al.* [20] was employed. In order to find the ground magnetic state, various magnetic configurations, such as AFM-G, AFM-A, AFM-C, and ferromagnetic (FM), were considered. For this purpose the unit cell was doubled along the **a** axis. For such a cell a k-point mesh of $4 \times 6 \times 2$ was chosen. The effective Hubbard U was varied from 2.5 to 4.5 eV, with J_H set to 1 eV. The total energy method was used to calculate the isotropic exchange interaction parameters. Spin-orbit coupling (SOC) was added to the calculation scheme to estimate the single-ion anisotropy.

The Néel temperature was computed by calculation of the temperature dependence of the specific heat simulated by the classical Monte Carlo method using the spinmc algorithm as realized in ALPS [21]. We used periodic boundary conditions on the $10 \times 10 \times 10$ box (and checked that a further increase of its length does not change the result) and 10 000 000 sweeps.

III. RESULTS AND DISCUSSION

A. Magnetic GGA+U calculations

It is well known that taking into account strong Coulomb correlations is essential to describe the electronic and magnetic properties of most of the transition metal oxides [8,22]. However, there is always a problem in estimating the interaction parameters. While substantial progress has been achieved
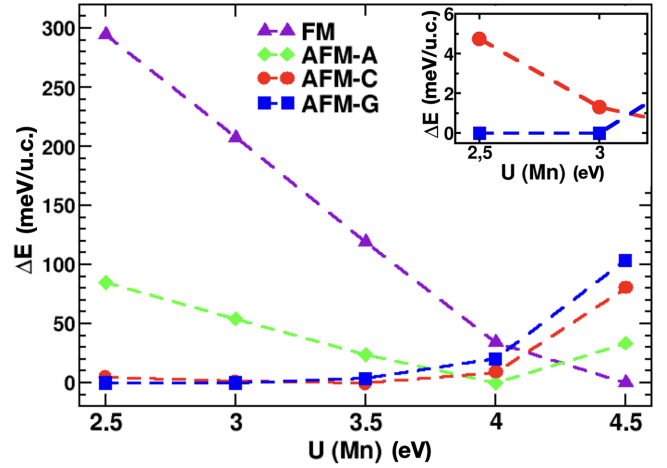
in recent years in this direction [23–25], there is still some arbitrariness in choosing Hubbard U. Therefore, we adopted another approach and performed a series of calculations for different U. In contrast to Hubbard U, Hund's intra-atomic exchange J_H can hardly be screened in solids (it is composed of several Slater integrals) and we took $J_H = 1$ eV as in many other studies [23,25].

There are three possible antiferromagnetic orders in the perovskite structure of HgMnO$_3$, in addition to the FM configuration. In the case of AFM-G type, each adjacent atom has oppositely directed magnetic moments (Néel AFM). Another configuration is AFM-C, in which there are antiferromagnetically ordered FM stripes running along the cubic **c** axis. The last AFM-A configuration corresponds to antiferromagnetically ordered FM planes.

Total energies of various magnetic configurations are presented in Fig. 2. As one can see, with increasing U, a gradual change of the ground magnetic state from a fully AFM (Néel) to pure FM is observed. In the case of $U = 2.5$ and 3 eV the lowest energy corresponds to the AFM-G state with all six nearest neighbors being AFM ordered. Further, increasing U up to 3.5 eV gives an AFM-C ground state with four antiferromagnetically and two ferromagnetically ordered nearest neighbors for each Mn. For the AFM-A structure being the ground state for $U = 4$ eV, each Mn has two neighbors with opposite spin orientation and four neighbors with codirectional magnetic moments. Finally, at $U = 4.5$ eV the ground magnetic state becomes FM. Thus, there is a clear tendency to increase the number of ferromagnetic bonds with growing U.

In order to choose the most reasonable U, we calculated the isotropic exchange interaction parameters for HgMnO$_3$ for different U values. The Heisenberg model is written in the following form,

$$H = \sum_{ij} J_{ij} \mathbf{S}_i \mathbf{S}_j, \qquad (1)$$

TABLE I. Parameters of the isotropic exchange interaction (in meV) calculated by the GGA+U approximation for various values of Hubbard U ($J_H = 1$ eV). In the last row, Curie-Weiss temperatures (in K) calculated by the mean-field approximation from these exchange parameters are presented.

J_{ij}	$U = 2.5$ eV	3.0 eV	3.5 eV	4.0 eV	4.5 eV
J_1	0.87	0.60	0.32	0.01	−0.35
J_2	0.24	0.18	0.12	0.05	−0.01
J_3	0.03	0.03	0.03	0.02	0.02
θ_{CW}	−241	−173	−104	−26	60

where the summation runs twice over each pair. Exchange paths between Mn atoms up to the third neighbors were considered [shown in Fig. 1(b)]. The results of the calculations are summarized in Table I and Fig. 3. As it was expected, the strongest exchange interaction was found to be between the nearest neighbors. It gradually decreases with U and finally changes sign, going from antiferromagnetic to ferromagnetic.

The Curie-Weiss temperature in the mean-field approximation, given by

$$\theta_{CW}^{MF} = -\frac{2S(S+1)}{3k_B} \sum_i Z_i J_i, \quad (2)$$

was estimated for each U (here, Z_i is the number of corresponding neighbors). One can see from Table I that the best agreement with the experiment is achieved for Hubbard $U = 3$ eV ($\theta_{CW}^{calc} = -173$ K and $\theta_{CW}^{expt} = -153$ K). Using J_1, J_2, and J_3 for the chosen Hubbard parameter $U = 3$ eV, one can recalculate the Néel temperature in the mean-field approximation as

$$T_N^{MF} = -\frac{2S(S+1)}{3k_B} J_{\mathbf{q}=\mathbf{Q}}, \quad (3)$$
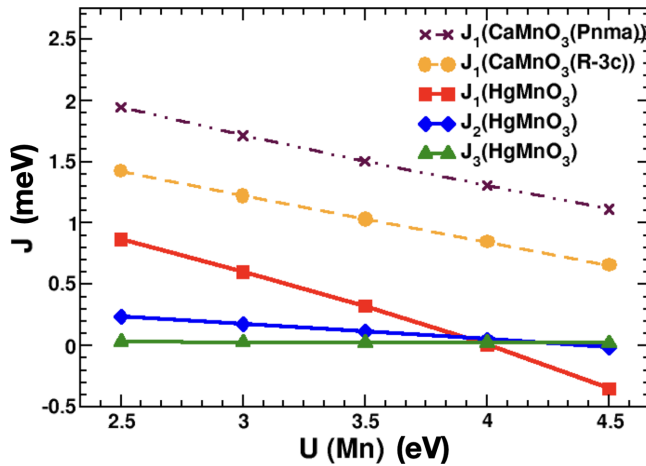
FIG. 3. Isotropic exchange interaction parameters (in meV) for various values of U ($J_H = 1$ eV). For comparison, calculated exchange interaction parameters J_1 for real CaMnO$_3$ (space group *Pnma*, shown in the dark purple dashed line) and for CaMnO$_3$ in the HgMnO$_3$ structure (shown in orange) are given.

with

$$J_{\mathbf{q}=\mathbf{Q}} = \min\left(\sum_j J_j e^{i\mathbf{a_j}\mathbf{q_j}}\right), \quad (4)$$

where $\mathbf{a_j}$ are corresponding lattice vectors and $\mathbf{Q}$ is the wave vector in reciprocal space at which J_q takes minimal values, $\mathbf{Q} = (\pi, \pi, \pi)$ in the case of $U = 3$ eV. It was found to be $T_N = 100$ K and it overestimates the experimental one ($T_N^{expt} = 60$ K) by approximately 1.5 times, which is typical for the mean-field approximation. Therefore, $U = 3$ eV seems to be a reasonable choice for the interaction parameter.

Already at this point one can notice a rather unexpected behavior of the exchange coupling between nearest neighbors J_1: It is not only much smaller than in the sister material CaMnO$_3$, but also changes sign, becoming ferromagnetic at large U, which is rather counterintuitive given the fact that the superexchange interaction between half-filled t_{2g} orbitals of Mn^{4+} must be antiferromagnetic. The origin of this anomaly is a large ferromagnetic contribution due to the electron transfer via Hg s states as we will demonstrate in Sec. III C. However, there is also another important factor, which leads to the suppression of the Néel temperature: frustration. An antiferromagnetic exchange interaction with next nearest neighbors, J_2, will frustrate the system and this effect cannot be treated by the mean-field method.

Therefore, we performed classical Monte Carlo (MC) simulations taking into account all three exchange parameters and also a single-ion anisotropy (SIA), which was estimated by the total energies in DFT+U+SOC calculations. Mn ions occupy $6b$ sites in the $R\bar{3}c$ structure, which correspond to the $\bar{3}$ point group with the C_3 axis pointing along the c axis. Calculating the total energies of configurations with spins directed along and perpendicular to the C_3 axis, we found that this is an easy axis, and the SIA constant D defined as

$$H_i^{SIA} = D\left(S_i^z\right)^2 \quad (5)$$

turns out to be -0.6 K for $U = 3$ eV. The resulting temperature dependence of the specific heat in MC calculations is presented in Fig. 4, and one can see that frustrations indeed suppress the Néel temperature leading to $T_N^{MC} = 48$ K. This is in line with the experiment, which shows moderate frustrations with the frustration index $|\theta_{CW}|/T_N \approx 2.6$.

Thus, one can see that $U = 3$ eV is a reasonable estimate of the interaction parameter, so all the following results will be given for this choice of Hubbard U. The ground magnetic state for $U \sim 3$ eV (or smaller, which probably would give even a closer estimation of T_N, but we do not pursue such an aim here) is AFM-G.

B. Electronic structure and altermagnetism

The calculated partial density of states (DOS) are given in Fig. 5. The calculated absolute value of the magnetic moment $\mu_{Mn} = 2.86 \, \mu_B$. As one can see, taking into account Coulomb and magnetic interactions immediately gives an insulating solution with a band gap of 0.72 eV (for $U = 3$ eV). The top of the valence band is formed by O $2p$ states, while the bottom of the conduction band mostly has Mn e_g character. As one
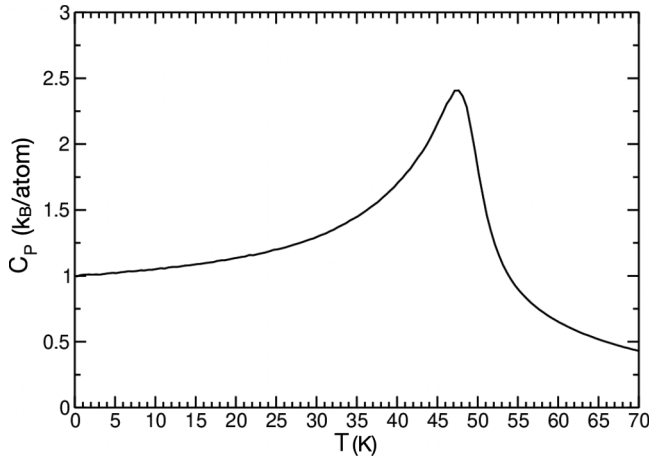
FIG. 4. Temperature dependence of the specific heat as obtained by the classical Monte Carlo simulations taking into account the classical to quantum renormalization factor [S^2 to $S(S+1)$] for exchange interaction parameters obtained in DFT+U calculations with $U = 3$ eV (and taking into account the single-ion anisotropy).

can see, not only empty Mn e_g (as expected) but also Hg s states lie rather close above the Fermi energy. This enables hybridization between these states, so they play a crucial role for the magnetism as we discuss in Sec. III C.

Next, we analyze the electronic structure of HgMnO$_3$ obtained for the ground state AFM-G order in detail. First, it has to be noticed that this magnetic order does not increase the primitive unit cell (with respect to the nonmagnetic situation), which consists of two formula units. Second, there is no inversion symmetry connecting two magnetic ions and, third, there is the C_2 axis, which transforms Mn from two different spin sublattices one into another. Therefore, HgMnO$_3$ is expected to be altermagnetic according to Ref. [26], i.e., there must
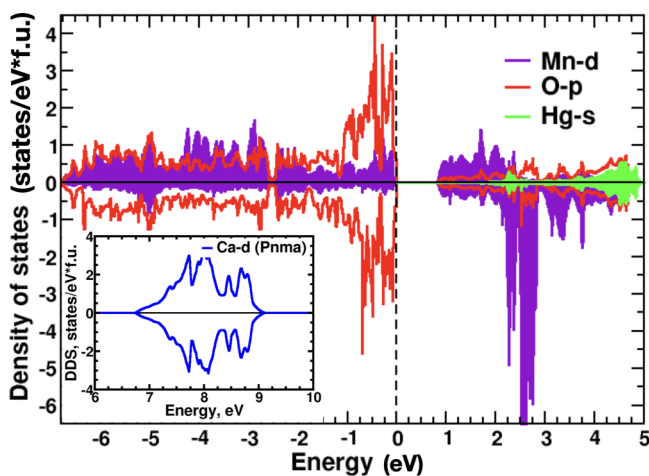
FIG. 5. The partial density of states (PDOS) per formula unit for HgMnO$_3$, calculated in the GGA+U approach with parameters $U = 3$ eV, $J_H = 1$ eV, for the AFM-G configuration (PDOS for Mn is given just for one type of atom). Positive and negative DOS corresponds to different spin projections. Position of Ca 3d in real CaMnO$_3$ is shown in the inset in blue. As one can see, they are significantly higher in energy than Hg s.
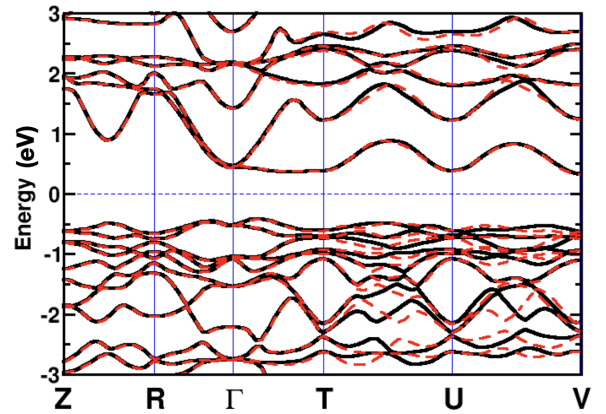
FIG. 6. Band structure for HgMnO$_3$ calculated in spin-polarized GGA+U ($U = 3$ eV, $J_H = 1$ eV). Black and red colors correspond to the bands for different spin projections, up and down, respectively. T, U, and V points are [0, 1/2, 1/2], [1/2, 0, 1/2], and [1/2, 1/2, 0].

be high-symmetry directions in the reciprocal space along which electronic bands for different spin projections do not coincide.

The band structure obtained in GGA+U calculations for the AFM-G configuration is presented in Fig. 6. As one can clearly see, bands from the opposite spin channels in the T-U direction (k vectors [0, 1/2, 1/2] and [1/2, 0, 1/2], correspondingly) do not lie on top of each other, both above and below the Fermi level. The same situation applies to the U-V direction. This fact directly demonstrates that HgMnO$_3$ is an altermagnet.

C. Mechanisms of exchange interaction

In fact, it is rather unusual that the Néel temperature for HgMnO$_3$ turns out to be as small as 60 K. Naively, for Mn^{4+} ions with all t_{2g} orbitals half filled, one would expect a strong antiferromagnetic exchange interaction according to the famous Goodenough-Kanamori-Anderson rules [22,27]. Moreover, ferromagnetic contributions typically have $1/U^2$ dependence, while antiferromagnetic ones have $1/U$ [28]. Therefore, the antiferromagnetic exchange should become smaller, but not change its sign for increasing U, if a conventional superexchange mechanism is operative in HgMnO$_3$. We see from Table I that this is in strong contrast to the results of direct GGA+U calculations. Indeed, above $U = 4$ eV the exchange constant J_1 between nearest neighbors becomes ferromagnetic. This suggests that another mechanism is decisive or at least contributes significantly to the total exchange.

In order to find out the origin of this anomaly we additionally calculated exchange parameters for CaMnO$_3$ and obtained that an exchange interaction with nearest neighbors, J_1 (a more detailed study of CaMnO$_3$ was performed in Ref. [29]), decreases slowly and never becomes FM (see Fig. 3, dark purple dashed line). Thus, we see that the exchange interaction in this material behaves in a conventional way and can be described by the superexchange mechanism. Next, we checked that the result is not related to the difference in volume and other details of the crystal structure between
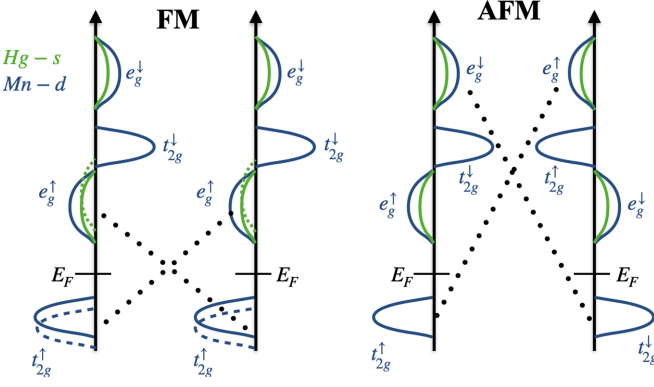
FIG. 7. Sketch illustrating the mechanism of the indirect exchange to explain the substantial ferromagnetic contribution in HgMnO$_3$. Left (right) corresponds to ferromagnetic (antiferromagnetic) ordering. Mn $3d$ states are shown by blue, while Hg $6s$ states by green solid lines. There is a hybridization (dotted line) between states of the same spin, which leads to a shift for the corresponding density of states. The result of hybridization is shown by dashed lines. One can see that it is more efficient in the case of the ferromagnetic configuration and therefore the indirect exchange via Hg $6s$ states will stabilize ferromagnetism.

Ca and Hg manganites. We replaced Hg ions by Ca ones in the $R\bar{3}c$ structure of HgMnO$_3$, recalculated J_1 for different U values, and also plot them in Fig. 3 by the orange dashed line. One can see that while J_1 decreased by an absolute value it has the same U dependence and never becomes FM as the nearest-neighbor exchange in real CaMnO$_3$. We also calculated all previously discussed isotropic exchange interaction parameters for $U = 3$ eV for CaMnO$_3$ in the $R\bar{3}c$ structure ($J_1 = 1.23$ meV, $J_2 = 0.17$ meV, and $J_3 = -0.01$ meV). For this case, the estimated by the mean-field approach Néel temperature immediately increases up to 213 K. Therefore, it is the Hg ions that lead the exchange interaction anomalies in HgMnO$_3$ and, consequently, this effect will influence the magnetic transition temperature.

In contrast to Ca, Hg ions have s states lying above the Fermi level (see Fig. 5). Being strongly hybridized with extended Mn e_g orbitals, these states can affect an exchange interaction via an indirect exchange mechanism, which is sketched in Fig. 7. This mechanism gives a FM contribution to the total exchange interaction. Indeed, hybridization between occupied spin majority t_{2g} states and empty Hg $6s$ states lower the t_{2g} band (and therefore decrease the total energy of this configuration) in the case of FM ordering between two Mn sublattices as illustrated in Fig. 7. Neglecting correlation effects, the corresponding energy decrease (due to the exchange interaction) is $\delta E_{\text{FM}} \sim \tilde{t}^2/\Delta_{\text{CFS}}$, where Δ_{CFS} is the crystal field $t_{2g} - e_g$ splitting (Hg $6s$ states are strongly hybridized with Mn e_g and placed at the same energy) and $\tilde{t}$ is the effective hopping between Mn d states via Hg $6s$ orbitals. In case of AFM ordering the hybridization will be with a much higher-lying states shifted by a Stoner splitting proportional to IM (I is the Stoner parameter and M is the sublattice magnetisation). Thus, for the AFM case the energy gain will be only $\delta E_{\text{AFM}} \sim \tilde{t}^2/(\Delta_{\text{CFS}} + IM)$. We see that this mechanism provides a FM contribution and in the first approximation it is independent on Hubbard U (in "atomic" language

it would rather depend on Hund's intra-atomic exchange). The corresponding contribution due to this indirect exchange (ie) via Hg $6s$ states is

$$J_{\text{ie}} = \frac{1}{4S^2}(\delta E_{\text{AFM}} - \delta E_{\text{FM}})$$

$$\sim -\sum_m \frac{IM\tilde{t}_m^2}{\Delta_{\text{CFS}}(\Delta_{\text{CFS}} + IM)}, \qquad (6)$$

where the summation runs over all possible hopping channels (between different orbitals). This FM contribution does not directly depend on U, but is rather scaled by Stoner I (or Hund's J_H as it was mentioned above). However, one may expect that by increasing U we shift empty Mn d states closer to empty Hg s states, making this mechanism even more efficient.

It is worthwhile mentioning that there is also a conventional FM superexchange between half-filled t_{2g} and empty e_g orbitals via orthogonal $2p$ orbitals as explained, e.g., in Ref. [30]. However, our GGA+U calculations of CaMnO$_3$ in the structure of HgMnO$_3$ clearly demonstrate that these are Hg s states, which are an essential ingredient for the suppression of the AFM exchange interaction.

IV. CONCLUSIONS

The results of our first-principles DFT calculations for both HgMnO$_3$ and CaMnO$_3$ compounds clearly show that these are not conventional modifications of the crystal structure that are responsible for the anomalous suppression of the Néel temperature in HgMnO$_3$. It turns out that the electronic structure of the A^{2+} site in A^{2+}Mn^{4+}O$_3$ manganites strongly affects the resulting exchange interaction and may cause the suppression of antiferromagnetism.

Presence of the Hg s states near the Fermi level and their hybridization with the Mn e_g subshell facilitates indirect exchange interaction, giving sizable ferromagnetic contribution in addition to the expected according to the Goodenough-Kanamori-Anderson rules antiferromagnetic exchange interaction. Experimentally, in the case of HgMnO$_3$ synthesized under high pressure the Néel temperature turns out to be two times smaller than in CaMnO$_3$. It has to be stressed that the physical mechanism lying behind suppression of the antiferromagnetic exchange interaction in HgMnO$_3$ is universal and can be applied for many other different materials containing ions with completely filled d states and empty s orbitals lying just above the Fermi level.

Last but not least, our analysis shows that HgMnO$_3$ is expected to be altermagnetic. This makes especially interesting studies of magneto-optical response as well as the spin-transfer torque in this highly unusual material [31].

[1] R. von Helmolt, J. Wecker, B. Holzapfel, L. Schultz, and K. Samwer, Giant negative magnetoresistance in perovskitelike La$_{2/3}$Ba$_{1/3}$MnO$_x$ ferromagnetic films, Phys. Rev. Lett. **71**, 2331 (1993).

[2] K. Chahara, T. Ohno, M. Kasai, and Y. Kozono, Magnetoresistance in magnetic manganese oxide with intrinsic antiferromagnetic spin structure, Appl. Phys. Lett. **63**, 1990 (1993).

[3] K. Uusi-Esko, J. Malm, N. Imamura, H. Yamauchi, and M. Karppinen, Characterization of RMnO$_3$ (R = Sc, Y, Dy-Lu): High-pressure synthesized metastable perovskites and their hexagonal precursor phases, Mater. Chem. Phys. **112**, 1029 (2008).

[4] M. Fiebig, T. Lottermoser, D. Fröhlich, A. V. Goltsev, and R. V. Pisarev, Observation of coupled magnetic and electric domains, Nature (London) **419**, 818 (2002).

[5] N. A. Hill and K. M. Rabe, First-principles investigation of ferromagnetism and ferroelectricity in bismuth manganite, Phys. Rev. B **59**, 8759 (1999).

[6] A. Sharan, J. Lettieri, Y. Jia, W. Tian, X. Pan, D. G. Schlom, and V. Gopalan, Bismuth manganite: A multiferroic with a large nonlinear optical response, Phys. Rev. B **69**, 214109 (2004).

[7] M. B. Salamon, M. Jaime, The physics of manganites: Structure and transport, Rev. Mod. Phys. **73**, 583 (2001).

[8] D. I. Khomskii and S. V. Streltsov, in *Encyclopedia of Condensed Matter Physics*, edited by T. Chakraborty, 2nd ed. (Academic, Oxford, UK, 2024), pp. 98–111.

[9] V. Markovich, A. Wisniewski, and H. Szymczak, in *Handbook of Magnetic Materials*, edited by K. H. J. Buschow (Elsevier, Amsterdam, 2014), Vol. 22, pp. 1–201.

[10] S. K. Mishra, M. K. Gupta, R. Mittal, A. I. Kolesnikov, and S. L. Chaplot, Spin-phonon coupling and high-pressure phase transitions of RMnO$_3$ (R=Ca and Pr): An inelastic neutron scattering and first-principles study, Phys. Rev. B **93**, 214306 (2016).

[11] N. T. Trang, B. T. Cong, Th.H. Thao, Ph. T. Tan, N. D. Tho, and H. N. Nhat, Magnetic state of the bulk, surface and nanoclusters of CaMnO$_3$: A DFT study, Phys. B: Condens. Matter **406**, 3613 (2011).

[12] J. Briático, B. Alascio, R. Allub, A. Butera, A. Caneiro, M. T. Causa, and M. Tovar, Double-exchange interaction in electron-doped CaMnO$_{3-\delta}$ perovskites, Phys. Rev. B **53**, 14020 (1996).

[13] B. Zhou, S. Qin, T. Ma, X. Ye, J. Guo, X. Yu, H.- J. Lin, C.-T. Chen, Z. Hu, L.-H. Tjeng, G. Zhou, C. Dong, and Y. Long, High-pressure synthesis of two polymorphic HgMnO$_3$ phases and distinct magnetism from 2D to 3D, Inorg. Chem. **59**, 3887 (2020).

[14] B. W. Zhou, J. Zhang, X. B. Ye, G. X. Liu, X. Xu, J. Wang, Z. H. Liu, L. Zhou, Z. Y. Liao, H. B. Yao, S. Xu, J. J. Shi, X. Shen, X. H. Yu, Z. W. Hu, H. J. Lin, C. T. Chen, X. G. Qiu, C. Dong, J. X. Zhang *et al.*, Octahedral distortion and displacement-type ferroelectricity with switchable photovoltaic effect in a $3d^3$-electron perovskite system, Phys. Rev. Lett. **130**, 146101 (2023).

[15] G. Kresse and J. Furthmüller, Efficiency of *ab-initio* total energy calculations for metals and semiconductors using a plane-wave basis set, Comput. Mater. Sci. **6**, 15 (1996).

[16] G. Kresse and J. Hafner, *Ab initio* molecular dynamics for liquid metals, Phys. Rev. B **47**, 558 (1993).

[17] G. Kresse and J. Furthmüller, Efficient iterative schemes for *ab initio* total-energy calculations using a plane-wave basis set, Phys. Rev. B **54**, 11169 (1996).

[18] J. P. Perdew, K. Burke, and M. Ernzerhof, Generalized gradient approximation made simple, Phys. Rev. Lett. **78**, 1396(E) (1997).

[19] P. E. Blöchl, O. Jepsen, and O. K. Andersen, Improved tetrahedron method for Brillouin-zone integrations, Phys. Rev. B **49**, 16223 (1994).

[20] A. I. Liechtenstein, V. I. Anisimov, and J. Zaanen, Density-functional theory and strong interactions: Orbital ordering in Mott-Hubbard insulators, Phys. Rev. B **52**, R5467 (1995).

[21] B. Bauer, L. D. Carr, H. G. Evertz, A. Feiguin, J. Freire, S. Fuchs, L. Gamper, J. Gukelberger, E. Gull, S. Guertler, A. Hehn, R. Igarashi, S. V. Isakov, D. Koop, P. N. Ma, P. Mates, H. Matsuo, O. Parcollet, G. Pawłowski, J. D. Picon, L. Pollet, E. Santos, V. W. Scarola, U. Schollwöck, C. Silva, B. Surer, S. Todo, S. Trebst, M. Troyer, M. L. Wall, P. Werner, and S. Wessel, The ALPS project release 2.0: Open source software for strongly correlated systems, J. Stat. Mech.: Theory Exp. (2011) P05001.

[22] D. I. Khomskii, *Transition Metal Compounds* (Cambridge University Press, Cambridge, UK, 2014).

[23] S. V. Streltsov, R. E. Ryltsev, and N. M. Chtchelkatchev, Ground-state structure, orbital ordering and metal-insulator transition in double-perovskite PrBaMn$_2$O$_6$, J. Alloys Compd. **912**, 165150 (2022).

[24] S. Zhang, J. Wang, T. Lei, X. Li, Y. Liu, F. Guo, J. Wang, W. Zhang, F. Dang, H. Seifert, L. Sun, and Y. Du, First-principles study of Mn antisite defect in Li$_2$MnO$_3$, J. Phys.: Condens. Matter **33**, 415201 (2021).

[25] K. Leung and C. J. Medforth, *Ab initio* molecular dynamics study of manganese porphine hydration and interaction with nitric oxide, J. Chem. Phys. **126**, 024501 (2007).

[26] L. Šmejkal, J. Sinova, and T. Jungwirth, Emerging research landscape of altermagnetism, Phys. Rev. X **12**, 040501 (2022).

[27] J. B. Goodenough, *Magnetism and the Chemical Bond* (Interscience Publishers, New York, 1963).

[28] D. I. Khomskii and S. V. Streltsov, Orbital effects in solids: Basics, recent progress, and opportunities, Chem. Rev. **121**, 2992 (2021).

[29] S. Keshavarz, Y. O. Kvashnin, D. C. M. Rodrigues, M. Pereiro, I. Di Marco, C. Autieri, L. Nordstrom, I. V. Solovyev, B. Sanyal, and O. Eriksson, Exchange interactions of CaMnO$_3$ in the bulk and at the surface, Phys. Rev. B **95**, 115120 (2017).

[30] S. V. Streltsov and D. I. Khomskii, Orbital physics in transition metal compounds: new trends, Phys. Usp. **60**, 1121 (2017).

[31] I. Mazin, Altermagnetism—A new punch line of fundamental magnetism, Phys. Rev. X **12**, 040002 (2022).